ELSEVIER

Journal of Nuclear Materials 266–269 (1999) 934–939

journal of nuclear materials

Comparison of scrape-off layer behaviour between DIV-I and DIV-II operations on ASDEX-Upgrade

J. Schweinzer *, W. Sandmann, G. Haas, J. Neuhauser, H. Murmann, H. Salzmann, ASDEX-Upgrade- and NBI-Teams

Max-Planck-Institut für Plasmaphysik, EURATOM Association, Boltzmannstr. 2, D-85748 Garching bei München, Germany

Abstract

The divertor geometry on ASDEX-Upgrade has changed from an open to a more closed configuration. The effects of this change on midplane scrape-off layer profiles for temperature and density are discussed. Investigations concerning the accuracy of separatrix positions are described. The relation between neutral gas flux density in the divertor and midplane density is analysed and scalings are presented. No decrease in the maximum achievable density in the H-mode with the new closed divertor in comparison to the former open one has been found. For comparable discharges the scrape-off layer density for the closed divertor has been found to be higher or at least as high as for the open divertor.

Keywords: ASDEX-Upgrade; Divertor

1. Introduction

One major goal of ASDEX-Upgrade (AUG) is to provide a basis for the design of the ITER divertor. Details of the design of the divertor chamber will significantly effect the performance of ITER as a consequence of the complex and non-linear interaction between plasma flow, neutral hydrogen and impurities. Predictions for ITER based on present model calculations only, seem not to be reliable enough. Therefore experimental investigations concerning critical divertor design elements are a necessary basis for the design of ITER. Changes in present divertor configurations will provide a particular discriminating testing ground for model approaches and will thus help to improve them considerably.

Therefore a new design based on extensive model calculations for the AUG Divertor-II (DIV-II) has been developed [1]. Divertor-II consists of two basic structures for the heat load carrying target plates, constructed in a modular form in order to allow within a short time the change of various elements and thus the divertor geometry.

In summer 97 ASDEX-Upgrade (AUG) has started operation with a new Lyra divertor (DIV-II) which is more closed and deeper than the former DIV-I configuration and is equipped with vertical inward directed target plates and a roof baffle in the private flux region. Fig. 1(a) and (b) shows a comparison between both divertor configurations.

A specific effect of the inward directed plates is that recycling neutrals will be directed towards the region of highest energy flux. From the modelled plasma circulation pattern a regime of high volumetric power losses from the most critical flux surfaces is expected, thus reducing the power load of plasma facing target plates to tolerable values. An improved AUG divertor was also demanded by the observation that the energy flux density on the AUG target plates has reached values close to the handling capabilities of DIV-I and the wish to increase the neutral beam heating power to 20 MW.

In this paper we will deal with the midplane scrape-off layer (SOL) and the plasma edge in DIV-I and DIV-II and will investigate differences caused by the change of the divertor. For this task we will make use of a SAS-formatted database which includes almost all

* Corresponding author. Tel.: +49 89 3299 1722; fax: +49 89 3299/2580; e-mail: jfs@ipp-garching.mpg.de.

0022-3115/99/$ – see front matter
PII: S0022-3115(98)00623-0

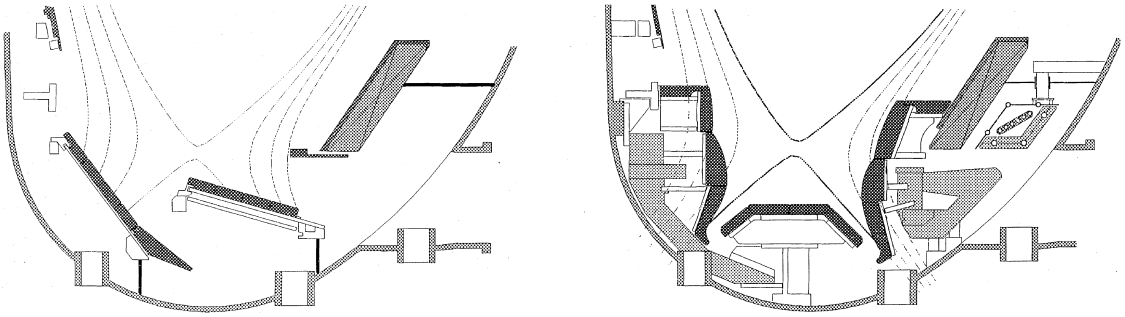

Fig. 1. (a) Poloidal cross-section of DIV-I; (b) Poloidal cross-section of DIV-II.

diagnostic information for various AUG discharges as well as compare 'identical' discharges of the DIV-I and DIV-II phase.

An overview about DIV-II and a comparison with results from B2/Eirene modelling as well as differences between DIV-I and DIV-II in power load to target plates and divertor radiation can be found in Refs. [2,3].

2. Position of separatrix R_{sep}

One major concern of investigations dealing with the plasma edge and the SOL is the radial position R_{sep} of the last close flux surface (separatrix). This position is determined at AUG by magnetics, which can be tested against a 1.5 D model for the temperature at R_{sep} [4,5] assuming classical parallel heat conduction between the midplane and the divertor. This model requires mainly an estimate for the power flow across the separatrix P_{SOL} and a high resolution T_e-profile (Fig. 2). Such a profile is obtained by overlaying a large number of T_e-profiles (Thomson scattering) measured in a plasma phase where the actual T_e-profile is assumed to be stationary. Small changes of the plasma position lead to an increased spatial resolution in comparison to a single measurement when the data points are plotted relative to the R_{sep} position of the magnetics (Fig. 2). This procedure assumes that the relative change of R_{sep} within the considered time interval (up to 1 s) is much more accurate than the absolute value.

Such a derived T_e-profile and the P_{SOL} value are the basis for a fitting procedure which determines R_{sep} and the transport coefficients of the assumed transport law. In Fig. 2 we compare two different fits ($n_e \cdot \chi_e = \text{constant}$ and $n_e \cdot \chi_e = c\ T_e$, $c \cdots$ constant) which both lead to very similar predictions for R_{sep} and are in very good agreement with the value from the magnetics.

For the DIV-I configuration an uncertainty of ±5 mm of R_{sep} was verified by application of these models to various discharges. The same process was now repeated for DIV-II showing a similar result, e.g. model predictions for R_{sep} and the magnetically defined values

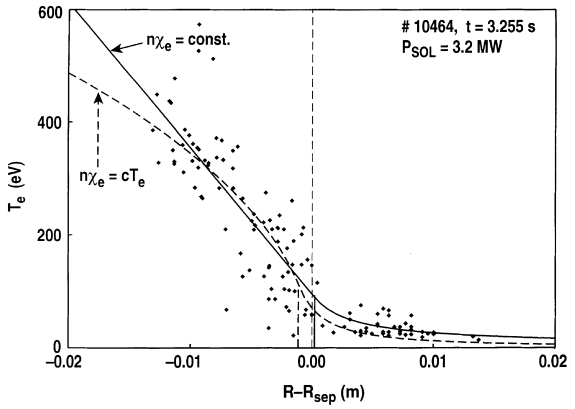

Fig. 2. T_e profile from edge Thomson scattering system (cf. text) for a H-mode discharge ($I_p = 0.8$ MA, $B_T = 2$ T, $P_{heat} = 5$ MW) with two T_e profiles from model calculations relative to the magnetically defined separatrix position. Resulting separatrix positions from the model calculations are indicated by vertical lines.

were within a few mm. Thus, the uncertainty of R_{sep} in both configurations is mostly about ±5 mm around the magnetically derived value.

3. Relation between the divertor neutral gas and SOL density profiles

The relation between neutral gas flux density Γ_0 in the divertor and midplane density profile parameters like n_e^{sep}, λ_{ne} and n_e^{SOL} has been of a rather general nature for DIV-I discharges [4]. Especially for the midplane averaged SOL density ($n_e^{SOL} = 1/L^{SOL} \cdot \int n_e(r)\, dr$; $L = 6$ cm) a robust relation $n_e^{SOL} \propto \Gamma_0^{0.5}\ q_{95}^{0.5}$ ($q_{95} \cdots$ safety factor) can be given which is of general validity for almost all operational regimes and different confinement modes like OH, L and H. For the latter averaging over ELMs is performed. The parameter n_e^{SOL} is introduced to gain a direct measure both for the transparency of the SOL plasma for neutral atoms and for the SOL thickness.

Systematic deviations from this general behaviour have been found for discharges with additional impurity puffs (Ne or N_2). In such cases with considerable impurity puff no dependency of n_e^{SOL} with Γ_0 is observed and n_e^{SOL} values are within a rather small range of $1.8–2.2 \times 10^{19}$ m^{-3} [4]. The break of the relation in such scenarios (CDH-mode) is attributed to complete divertor detachment where the power flow to the target plates practically vanishes and n_e^{SOL} becomes decoupled from the density of divertor neutrals.

For DIV-II a position of the pressure gauge in the private flux region has been chosen, which should deliver a measurement of the neutral gas flux density which can be compared to the one of DIV-I. For a series of five clean DIV-II H-mode discharges ($I_p = 0.6–1.2$ MA, $B_T = 2–2.5$ T, $P_{NBI} = 5$ MW, with density ramp-up near H→L transition) a similar scaling relation $n_e^{SOL} \propto \Gamma_0^{0.5} \cdot q_{95}^{0.968}$ has been found. In comparison to DIV-I only the q_{95} dependence is more pronounced. The former regression analysis for DIV-I (above scaling relation for n_e^{SOL}) used a Γ_0 measurement on a different position outside the outer strike zone which might be the reason for the differences in the dependence on the safety factor. Applying this scaling to both DIV-I and DIV-II data is shown in Fig. 3 and shows that midplane n_e^{SOL} is rather good described by one relation only for both divertor geometries. Very high values of Γ_0 have been obtained for DIV-I by reducing the neutral pumping rates by switching off some of the 14 turbo molecular pumps (TP). These discharges are marked in Fig. 3 by the symbol x and show stronger deviation from the scaling, because the reduction of the number of active TPs introduces a toroidal unsymmetry in the divertor Γ_0 value. With all 14 TPs active (pumping efficiency ≈14 m^3 s^{-1}) data from two gauges in the private flux region on different toroidal positions differ by 10–30%, whereas in the case of only 3 active TPs the differences at these two locations can be up to a factor of 3, which introduces a considerable uncertainty in the determination of the 'average' Γ_0 and leads therefore to the increased scatter in Fig. 3

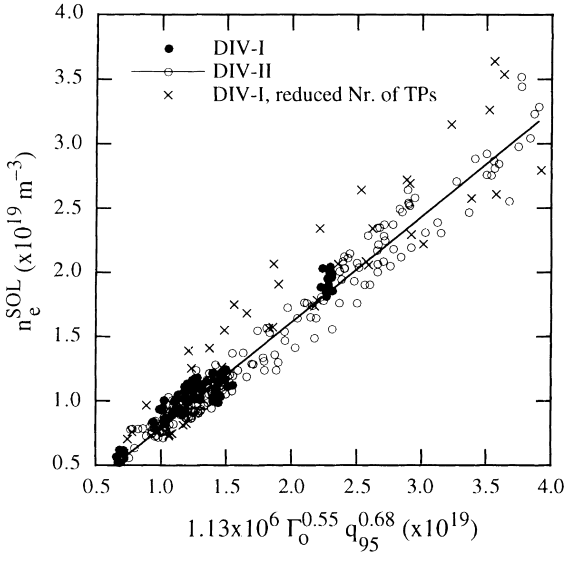

Fig. 3. Line averaged SOL density n_e^{SOL} vs. the result of a regression analysis (cf. text) for deuterium discharges of DIV-I and DIV-II phases.

4. SOL fall-off lengths of density and temperature

A rather good ordering of fall-off lengths can be achieved by using the energy confinement time τ_E. Temperature fall-off lengths λ_{T_e} are determined within a range of ±0.25 cm around the separatrix ($\lambda_{T_e} = T_e/T_e'$) whereas the density fall-off length λ_{ne} is determined by fitting an exponential function to the profile in the radial range [R_{sep}, R_{sep} + 2] cm.

Averaging over ELMs is performed. Between ELMs the λ_{ne} value is reduced by 20–40%. Fall-off lengths for both temperature and density are within error bars very similar in DIV-I and DIV-II. For both geometries λ_{ne} is 3–4 times larger than λ_{T_e} (Fig. 4).

The approach to determine the separatrix position (Section 2) delivers even smaller λ_{T_e} values (3–4 mm for H-modes with low to moderate gas puff) at the model-predicted separatrix position in comparison to the ones of Fig. 4.

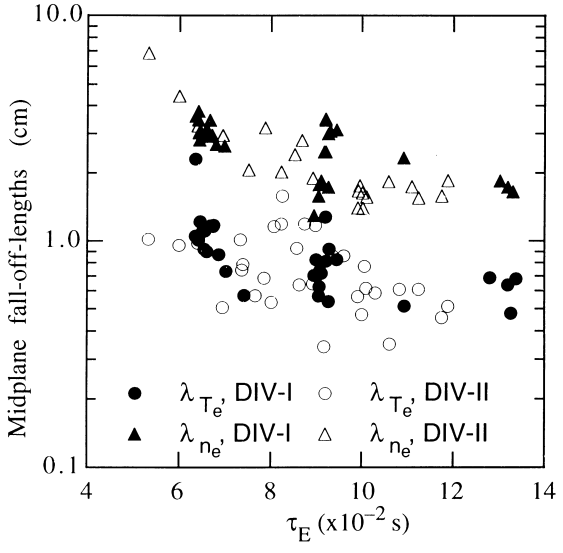

Fig. 4. ELM averaged SOL fall-off lengths for temperature and density. DIV-I: H-mode dataset with $I_p = 0.6–1.2$ MA, $B_T = -2.5$ T, $P_{heat} = 4.7–5.3$ MW and moderate gas puffing; DIV-II: H-mode dataset with $I_p = 0.6–1.0$ MA, $B_T = -2.5$ T, $P_{heat} = 4.8–5.2$ MW, with and without gas puffing.

Although the scattering is rather large a decrease of fall-off lengths with increasing energy confinement is observed. The pressure gradient in the H-mode transport barrier is known to be related with the quality of confinement [6]. This relationship is still found in the SOL region where radial transport is in strong competition with the particle flow along field lines towards the divertor and thus the pressure profile is rapidly decaying (in good approximation with λ_{T_e}).

The observed broadening of the divertor power flux profile [2,3] is not accompanied by larger fall-off lengths of the midplane profiles. The change of the divertor profiles between DIV-I and DIV-II is therefore caused by effects in the divertor region only (cf. details [2,3]).

5. H-mode density limit

The H-mode with ELMs is still regarded as the most promising stationary regime of enhanced confinement for a future reactor-size fusion device. The maximum achievable line averaged density in H-mode DIV-I discharges has been limited by a H→L transition and reached only 80–90% of the empirical Greenwald density limit [7]. Attempts to overcome this value by strong gas puff accompanied with high NBI heating power did not succeed. Near the H→L transition a saturation of n_e was observed, whereas n_e^{SOL} still was rising corresponding to increasing Γ_0 caused by the gas puffing. Most unwanted a considerable degradation in H-mode confinement with increasing density has been found.

In the following we compare two "identical" discharges from DIV-I and DIV-II with the same global parameters ($I_p = 0.8$ MA, $B_T = -2$ T, $q_{95} = 4$, 7.5 MW neutral beam heating) where the density is ramped up by gas puffing (2 active main chamber valves in both cases, maximum puffing rate 1.0×10^{22} s^{-1} applied near the H→L transition).

Very similar n_e values of 8.4×10^{19} m^{-3} are reached in both divertor geometries near the H→L transition. Corresponding Γ_0 values in the divertor are also the same, but higher midplane neutral gas flux density is measured for DIV-I (Fig. 5). An interesting point to note is that near the H→L transition the same Γ_0 value is reached in both geometries at the same gas puff rate and only 3 TPs active for DIV-I and 10 TPs active for DIV-II. The more open configuration of DIV-I required the shut-down of 11 TPs in order to reach such high Γ_0 values. For lower $n_e\Gamma_0$ in DIV-II is always higher than in the DIV-I configuration.

In Fig. 6 line averaged density n_e and separatrix and SOL density are plotted vs. the square root of Γ_0 (Section 3). For same Γ_0 within errors the same edge densities are found in DIV-I and DIV-II – as expected from the findings in Section 2 – but considerably lower line averaged densities except near the highest values near the H→L transition.

The different behaviour of edge densities in relation to the global line averaged one can also be observed by plotting the ratio n_e^{sep}/n_e (Fig. 7). For DIV-I, values

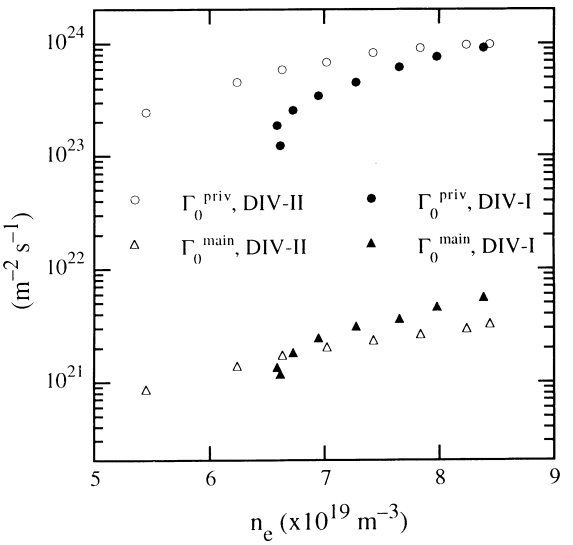

Fig. 5. Neutral gas flux densities measured in the private flux region and in the midplane for two similar density ramp-up discharges of DIV-I (#8383, 3 active TPs) and DIV-II (#10046, 10 active TPs). Discharge parameters: $I_p = 0.8$ MA, $B_T = -2$ T, $P_{heat} = 7.5$ MW.

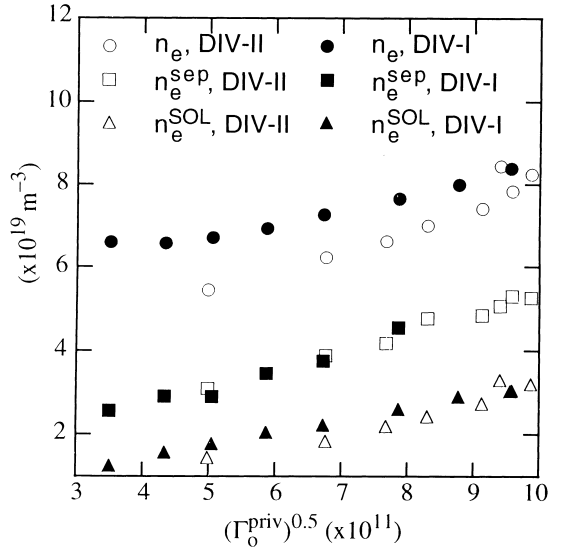

Fig. 6. Comparison of line averaged, SOL and separatrix density in two similar density ramp-up discharges of DIV-I (#8383, 3 active TPs) and DIV-II (#10046, 10 active TPs). Discharge parameters: $I_p = 0.8$ MA, $B_T = -2$ T, $P_{heat} = 7.5$ MW.

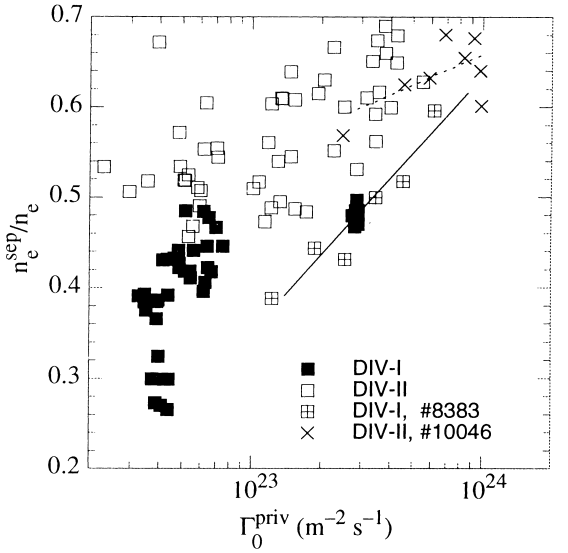

Fig. 7. Comparison of SOL and separatrix density in two similar density ramp-up discharges of DIV-I (#8383, 3 active TPs) and DIV-II (#10046, 10 active TPs). Discharge parameters: $I_p = 0.8$ MA, $B_T = -2$ T, $P_{heat} = 7.5$ MW.

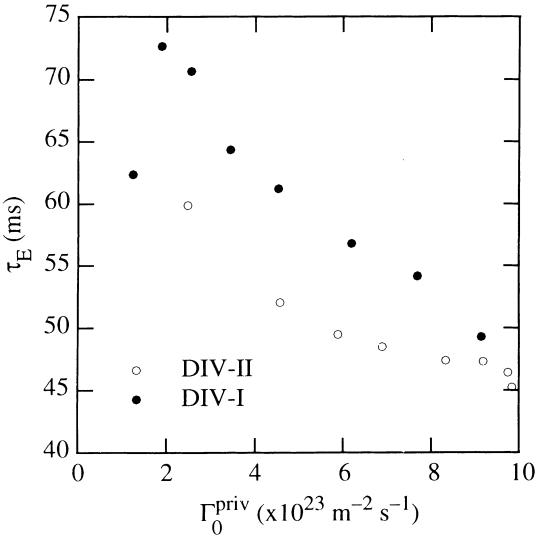

Fig. 8. Global energy confinement time τ_E of two similar density ramp-up discharges of DIV-I (#8383, 3 active TPs) and DIV-II (#10046, 10 active TPs). Discharge parameters: $I_p = 0.8$ MA, $B_T = -2$ T, $P_{heat} = 7.5$ MW.

between 0.25 and 0.6 occur and this ration is clearly a function of Γ_0 (cf. # 8383 in Fig. 7). In contrast, almost no values below 0.5 are found for DIV-II. High central density at low n_e^{sep} values does not seem to occur in DIV-II. This result is not only restricted to H-modes but is also true for OH and L-modes.

The plasma stored energy time is found to decrease with increasing density or equivalent with neutral divertor gas flux density pointing to a considerable degradation of confinement when the density is raised towards the H→L transition. For both divertor geometries this effect observed is rather similar. Especially near the H→L transition almost no difference is found in τ_E. (Fig. 8) However, for lower Γ_0 values τ_E in DIV-I is larger than in DIV-II. This difference is most probably due to changes in the core MHD behaviour which for DIV-II discharges is characterised by more pronounced sawtooth, fishbones and neo-classical tearing mode activity especially at low densities. The change of MHD behaviour caused by different divertor geometries seems to be rather unlikely, however, all other changes on AUG accompanied with the change from DIV-I to DIV-II are apparently small. One possible explanation could be the slightly increased plasma triangularity, but a satisfactory explanation is still missing.

6. H-mode power threshold

The H-mode power $P_{L\to H}$ threshold is known to scale with global parameters as $P_{L\to H} \propto n_e \cdot B_T$. A clear higher threshold (≈20%) is found for DIV-II in a limited number of comparable deutrium discharges [8] The reason for this increase might be due to the increased edge density when two discharges with the same line averaged density are compared. Using n_e^{sep} instead of n_e in the scaling for $P_{L\to H}$ would most probably lead to a reduced or even vanishing difference. However, a scaling attempt with statistical significance using edge density is still missing.

7. Summary and conclusions

The relation between SOL density and neutral gas flux density in the divertor is not significantly altered by the change from DIV-I to DIV-II. The ratio between line averaged density and separatrix density at high recycling near the H→L back transition is also not changed between DIV-I and DIV-II. However, discharges with low or even closed gas puff exhibit in DIV-II considerably higher SOL densities in relation to the line averaged one than in DIV-I. Thus the thickness of the SOL is under all conditions increased or at least the same as for DIV-I increasing the screening ability of the SOL plasma for penetrating neutrals. In addition the neutral main chamber density is similar or even slightly reduced in DIV-II for a given n_e. However, less neutrals in the main chamber and their better screening by the thicker SOL in DIV-II did not improve the H-mode confinement. This observation suggests, that neutrals penetrating the SOL to the H-mode transport barrier are

not the fundamental reason for H-mode confinement degradation.

The H-mode power threshold is about 20% higher in DIV-II than in DIV-I. Similar fall-off lengths for both T_e and n_e and thus p_e are found for DIV-I and DIV-II

References

[1] H.S. Bosch et al., IPP-report 1/281a (1994).
[2] R. Schneider et al., these Proceedings.
[3] A. Hermann et al., these Proceedings.
[4] M. Keilhacker et al., Phys. Scripta T2(2) (1982) 443.
[5] J. Schweinzer et al., Proceedings of the 24th European Conference on Plasma Physics and Controlled Fusion, Berchtesgaden, European Physical Society, to be published.
[6] W. Suttrop et al., these conference.
[7] V. Mertens et al., 16th IAEA Fusion Energy Conference, Montreal, 1996; International Atomic Energy Agency, Vienna, 1997, IAEA-F1-CN-64/A4-4.
[8] J. Neuhauser, IPP-report 1/311 (1997).